Experimental Study of Oscillation of Axisymmetric Turbulent Opposed Jets with Modulated Airflow

Wei-Feng Li, Guo-Feng Huang, Gong-Yi Tu, Hai-Feng Liu, and Fu-Chen Wang
Key Laboratory of Coal Gasification and Energy Chemical Engineering of Ministry of Education, Energy Chemical Engineering Dept., East China University of Science and Technology, Shanghai 200237, China

DOI 10.1002/aic.14190
Published online July 23, 2013 in Wiley Online Library (wileyonlinelibrary.com)

Oscillation behaviors of axisymmetric opposed jets with modulated airflow were experimentally studied. The oscillation frequency, the oscillation amplitude, and the movement velocity of the impingement plane at various nozzle separations, excitation frequencies, and exit turbulence intensities have been investigated by a hot-wire anemometer and flow visualization technique combined with a high-speed camera. Results show that the oscillation frequency of the impingement plane is nearly equal to the excitation frequency, whereas the oscillation amplitude decreases with the increase of the excitation frequency. The full-scale amplitude oscillation occurs at low excitation frequencies and $2 \leq L/D \leq 8$ (where L is the nozzle separation and D is the diameter of the nozzle exit). With the increase of the exit turbulence intensity caused by a turbulence generating plate, the oscillation amplitude decreases remarkably. Flow regimes of axisymmetric opposed jets with excitations are analyzed and discussed based on the experimental results. © 2013 American Institute of Chemical Engineers *AIChE J*, 59: 4828–4838, 2013
Keywords: fluid mechanics, mass-transfer

Introduction

Impinging streams is a unique and multipurpose flow configuration, which was first proposed by Elperin and further developed by Tamir.[1,2] As impinging jet flows can intensify transfer and mixing processes effectively, they has been widely and successfully applied to more and more industrial processes, for example, reaction injection molding (RIM), opposed multiple burners gasification, combustion, extraction, absorption, drying, and nanoparticle synthesis. However, the fundamental study of impinging jets is still very limited and imperfect in comparison with the increasing industrial applications.

For axisymmetric opposed jets, the flow instability is a very interesting and crucial issue, which has been observed by many researchers at various nozzle separations, exit Reynolds numbers, and boundary conditions, and evidently different types of instability behaviors have been reported. The first instability regime of opposed jets is the stagnation point offset. Several researchers have observed that it was very difficult to get the stagnation point to locate at the midpoint of the turbulent opposed jets at given experimental conditions.[3–9] The stagnation point offset of turbulent opposed jets has been extensively studied in our previous study.[10–12] We have found that there exists a range of $2D \leq L \leq 8D$, in which the stagnation point is very sensitive to the exit velocity ratio of the opposed jets. Simulations and bifurcation analyses of the structure and stability show that laminar axisymmetric opposed jets exhibit three steady states (two stable steady states and one unstable steady state) about at $Re > 60$, and no oscillatory instabilities were reported.[13,14]

Unlike to the stagnation point offset, other researchers observed many types of oscillation behaviors for axisymmetric opposed jets. For the flow in RIM, the transition from stable laminar to chaotic oscillation have been reported at $Re \approx 100$ and the Strouhal number (St) is in the range of 0.004–0.06 at $100 < Re < 250$.[15–17] At $250 < Re < 600$, the flow in RIM shows a self-sustained chaotic oscillation, and its St is about 0.04 and is found to be determined by the geometry configuration of mixing chamber.[18,19] However, Stan and Johnson[20] have observed an irregular low-frequency oscillation (1–20 Hz) for two opposed water jets, and the corresponding values of St are in the range of 2–8. In our previous study,[21] we have also observed some axial irregular oscillations or quasiperiodic oscillations for unrestricted axisymmetric opposed jets occasionally, whose peak frequency is about 10 Hz and St is in the range of 0.01–0.07. It should be pointed out that the irregular oscillation or quasiperiodic oscillation result form the exterior disturbances such as the flow fluctuation or smoke-wires. It can be seen that the oscillation regimes of unrestricted axisymmetric opposed jets are basically different to the self-sustained oscillation in RIM and the periodic deflecting oscillation of planar opposed jets.[21–23]

The excitation of modulated inflow has been widely used in the fluid mixing,[24,25] particle dispersion,[26] and liquid breakup.[27] However, the study of the flow regime of axisymmeric opposed jets with excitation is very rare, although it is important to fundamental fluid dynamics and applications. On one hand, the study of opposed jets with excitation is

Correspondence concerning this article should be addressed to W.-F. Li at liweif@ecust.edu.cn.

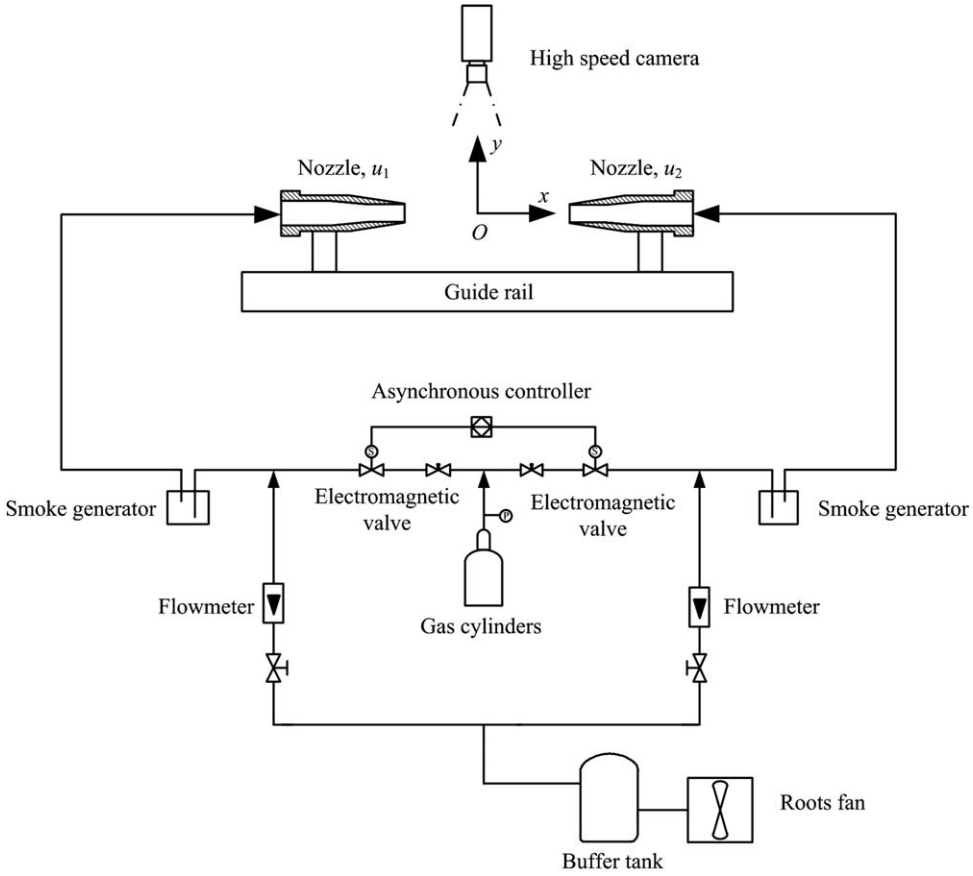

Figure 1. Schematic of experimental setup.

very important to further disclose the flow instability, as the modulation of inflow can be regarded as a periodic disturbance imposed on the flow system. On the other hand, turbulent opposed jets with modulation can be used to improve the mixing performance and enhance the heat- and mass-transfer rate in impinging jet reactors.

For microchannel devices, excited opposed jets have been used to enhance the mixing in recent years.[28,29] Erkoç et al.[30] have performed numerical simulations to study the effect of pulsation on the flow dynamics of a two-dimensional (2-D) laminar T-jets mixer, and found the oscillation amplitude of the pulsation has a strong effect on the flow. Icardi et al.[31] have investigated the flow field in a 3-D confined impinging jets reactor by means of micro Particle Image Velocimetry (microPIV) and Direct Numerical Simulation (DNS). They have found that oscillations present in the inlet flow of the device are in fact primarily responsible for the chaotic and turbulent effects in the reactor, and some small excitation oscillations similar to the experimental ones should be introduced in inflow conditions in DNS. Qiu et al.[32] have presented a 2-D simulation of the mixing characteristics of laminar opposed jets, and proved the periodic oscillation induced by pulsation is an effective way to improve mixing performance of laminar impinging jets. Though excitations of opposed jets have been applied in active mixing devices and numerically simulated to investigate the mixing enhancement, the oscillation regimes of axisymmetric opposed jets under excitations have not been revealed yet.

Motivated by the contributions of above studies, we present a fundamental study of the oscillation of axisymmetric turbulent opposed jets with excitations of modulated airflow in this article. Current study for the first time presents the flow regime of axisymmetric turbulent opposed jets with excitation, which is characterized by a periodic oscillation of the impinging plane along the symmetric axis. This excited oscillation is induced by the asynchronous velocity fluctuations in the inlets of the opposed jets and synchronizes with the excitation. In current article, our objectives are to identify the oscillation behaviors of turbulent opposed jets under excitations, and to propose a method to enhance the mixing of axisymmetric opposed jets.

Experimental Methods

Experiment setup

The schematic setup is drawn in Figure 1. Air was supplied by a Roots blower and buffered in a tank to eliminate the low-frequency influence of the vane of the blower. The atmospheric temperature and pressure in the experiments were 20°C and 100.72 kPa, respectively. The bulk fluxes of the airflow from the buffer tank were controlled by two rotameters with accuracy of $\pm 1\%$ of full-scale deflection. The turbulent flow field of opposed jets was obtained by two axisymmetric nozzles with equal geometric configurations. The opposing nozzles were precisely aligned in a guide rail to adjust their separation (L). The exit diameters (D) of the nozzles were 10 ± 0.02 mm and the normalized nozzle separations (L/D) were in the range of 1–20. The bulk mean velocities (u_0) at the nozzle exits were in the range of

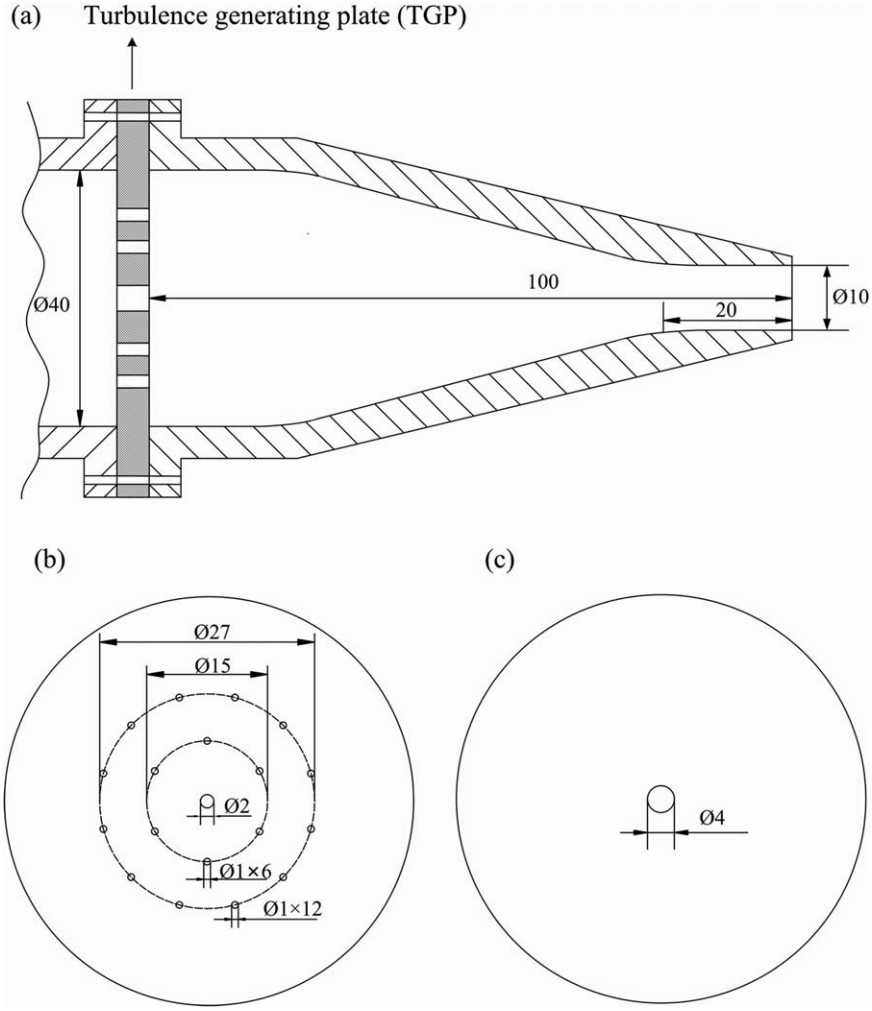

Figure 2. Cross-section of the axisymmetric nozzle (a), type A (b), and type B (c) turbulence generating plate with all dimensions in millimeters.

1.42–9.91 m/s, and the corresponding jet Reynolds numbers ($Du_0\rho/\mu$) were in the range of 946–6624.

As shown in Figure 1, the base flow was supplied by the blower and the pulsed air was added to the base flow. The additional air from the steel cylinder was controlled by two electromagnetic valves with a very short response time (less than 5 ms). The modulated airflow was generated and controlled by the periodic open and close of the electromagnetic valves, which were controlled by an asynchronous controller to adjust the phase displacement of the instantaneous velocity waveforms of the opposed jets. In current experiment, the phase displacement was set to π. The excitation frequency (f_0) was in the range of 0.5–25 Hz. The excitation amplitude (A_0) of the modulated airflow was changed by adjusting the outlet pressure of the gas cylinder and was determined by measuring the velocity fluctuation at the center of the nozzle exit with a hot-wire anemometer. The ratios (A_0/u_0) of the excitation amplitude of the pulsed gas to the base flow were about 10 and 20%, respectively.

The dimensions of the nozzle are plotted in Figure 2a. Two types (denoted by type A and type B) of turbulence generating plates (TGP) with high-blockage ratios were also used to generate higher turbulence intensity,[9,33] as drawn in Figures 2b, c.

Flow visualization

The instantaneous flow patterns of opposed jets were visualized by some white smoke generated by some small fuming tablets, which were composed of sawdust (20%), $KClO_3$ (20%), KNO_3 (15%), $(NH_4)_2SO_4$ (10%), and clay (35%). As shown in Figure 1, the tablets were placed in the smoke generators and the generated smoke was carried into the flow field. In the experiment, the smoke can be introduced to only one jet to observe the shape and location of the impingement plane more clearly. A high-speed camera (Photron, APX-RS, up to 3000 frames per second with full resolution of 1024 $\times$ 1024 pixels) combined with a continuous 2000 W direct current light were used to capture the instantaneous images of the smoke-seeded flow. The exposure time was set to 0.001 s, and the instantaneous images were photographed with a frame rate of 1000 frames per second and resolution of 1024 $\times$ 1024 pixels. The recording time of the high-speed camera depended on duration of the fuming tablet, which was about 1 min and covered at least 30 oscillation periods of the impingement plane for each experimental condition. The summary of the experimental cases of the flow visualization is listed in Table 1.

The recorded digital images were analyzed with the NIH Image freeware. Because the flow pattern of the recorded digital image was zoomed in, a simple conversion was

Table 1. Summary of Experimental Conditions and Parameters

Item	Symbol	Value
Inner diameter at the nozzle exit (mm)	D	10
Normalized nozzle separation	L/D	1–20
Mean bulk velocity at the nozzle exit (m/s)	u_0	1.42–9.91
Jet Reynolds number	Re	946–6624
Excitation frequency (Hz)	f_0	0.5–25
Relative excitation amplitude	A_0/u_0	10%, 20%
Phase displacement of two pulsed jets	Φ	π

needed. As shown in Figure 3, the nozzle separation in the image (L') was measured as the length scale, and the distances from the left nozzle exit to the impingement plane (x'_i) at time i were also measured, so the normalized coordinate (x_i/L) can be described as

$$x_i/L = x'_i/L' - 1/2 \tag{1}$$

where x_i is the real axial coordinate of the impinging plane referring to the origin in the reference frame as shown in Figure 1, and L is the real nozzle separation. Then, the mean movement velocity of the impingement planes (u_{ip}) at an interval of Δt can be defined as

$$u_{ip} = (x_{i+\Delta t} - x_i)/\Delta t \tag{2}$$

where Δt can be times of 0.001 s.

The oscillation period (T) is defined as the time interval during which the impinging plane finishes a reciprocating motion between the nozzle exits. By fast Fourier transform (FFT), the oscillation frequencies (f) can also be obtained from the time series of the locations of the impinging plane. The oscillation amplitude (A) of the impingement planes can be described as

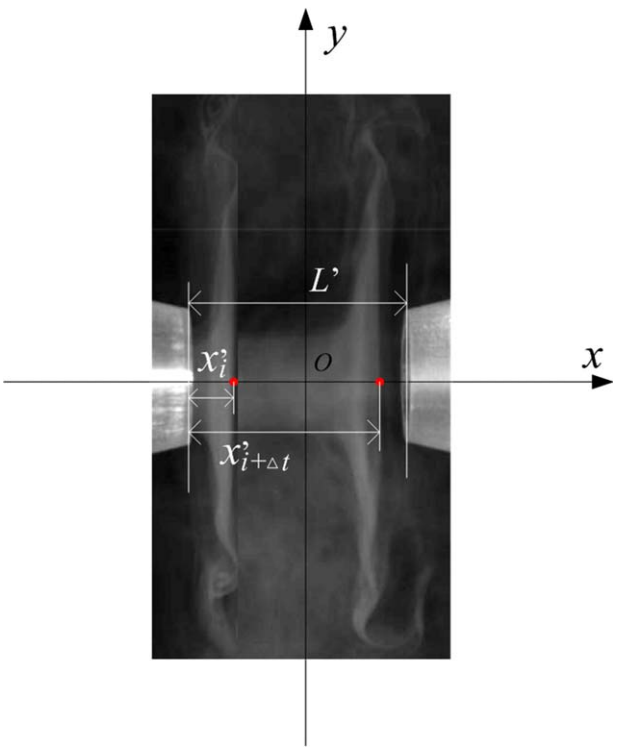

Figure 3. Schematic of image analysis.

[Color figure can be viewed in the online issue, which is available at wileyonlinelibrary.com.]

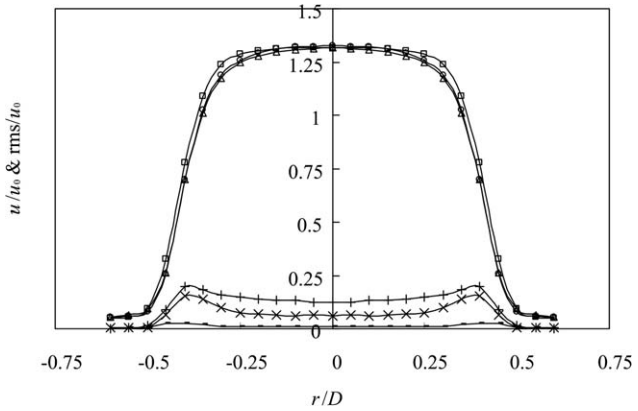

Figure 4. Exit axial velocity and turbulence intensity profiles of free jets at *Re* = 946.

Axial mean velocity: □, without TGP; ○, type A TGP; Δ, type B TGP. Turbulence intensity: -, without TGP; ×, type A TGP; +, type B TGP.

$$A = x_{\max} - x_{\min} \tag{3}$$

where $x_{\max}$ and $x_{\min}$ are the maximum and minimum coordinates in an oscillation period.

Hot-wire anemometer measurements

The axial mean and root mean square (rms) velocities at the exit (2 mm away from the nozzle exit) of the free and single jet were measured by a hot-wire anemometer system (DANTEC, Streamline 4). The sampling probe (DANTEC, 55P11, Pt, 5 μm diameter) of the hot-wire anemometer had a single wire. The probe was installed in a 3-D coordinate frame and the uncertainty of positioning was ±0.1 mm. The sampling frequency was set to 10 kHz and the sampling duration was 5 s. The total uncertainty of the velocity calibration, acquiring conversion of the hot-wire anemometer,

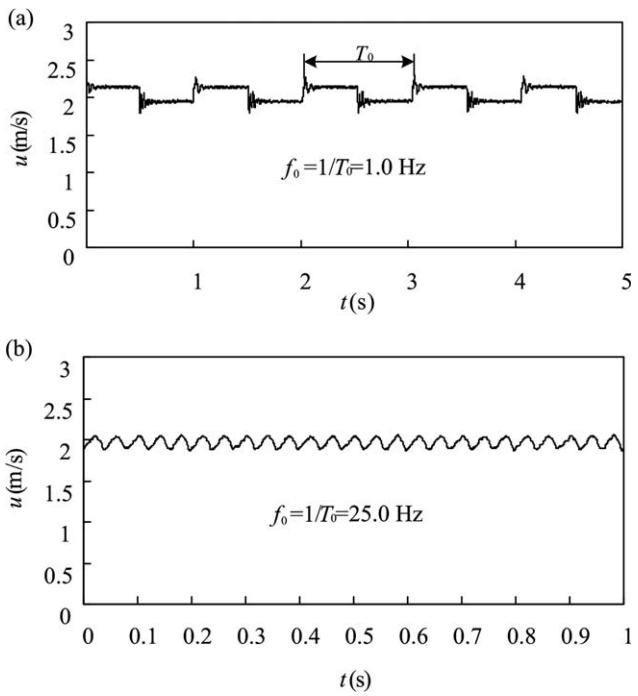

Figure 5. Time series of axial velocities at the center of nozzle exits at *Re* = 1892.

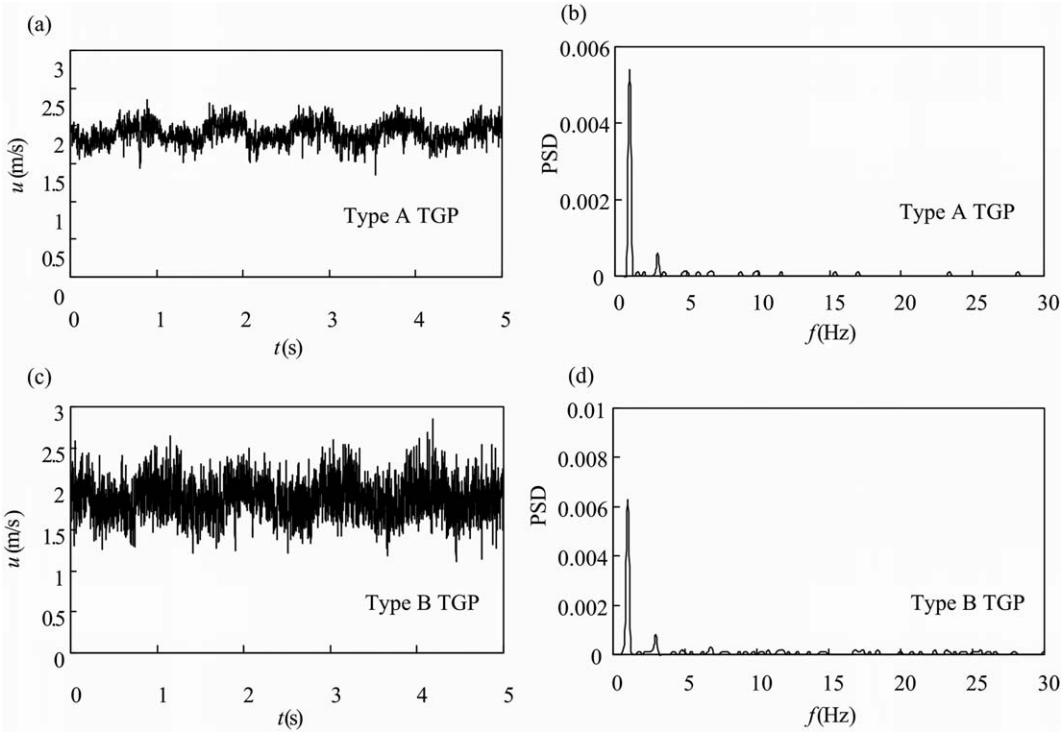

Figure 6. Time series and power-frequency spectra of axial velocities at center of jet exit with turbulence generating plate at $Re = 1892$ and $f_0 = 1.0$ Hz.

was less than 3%.[34] The reproducibility of the measurements of axial mean and rms velocities was determined by repeating a point measurement 10 times, and the yielded standard deviations were less than 5%.

At $Re = 946$, the measurements of axial mean and rms velocities are presented in Figure 4. All the axial velocity profiles are top-hat-shaped even with higher exit turbulence intensities. The central turbulence intensities at the nozzle exits corresponding to cases of no TGP, with type A and B TGP are about 1.1, 6.0, and 12.4%, respectively.

The time series of axial velocities at center of nozzle exits with various excitation frequencies and excitation amplitudes were measured by the hot-wire anemometer. At $f_0 < 5$ Hz, the instantaneous velocity curve is like a square wave, as shown in Figure 5a; whereas at $f_0 > 5$ Hz, the instantaneous velocity curve becomes like a sinusoidal wave, as shown in Figure 5b. The change of curve shapes from the square wave to sinusoidal wave is caused by the influence of the valve action time on the airflow at high excitation frequencies. For opposed jets formed by two excited jets with square waveforms, the instantaneous velocity can be approximately expressed as

$$\begin{cases} u_1 = u_0 + A_0 \\ \qquad\qquad , \quad 0 < t \le T_0/2, \quad \text{and} \\ u_2 = u_0 \end{cases} \tag{4}$$

$$\begin{cases} u_1 = u_0 \\ \qquad\qquad , \quad T_0/2 < t \le T_0 \\ u_2 = u_0 + A_0 \end{cases}$$

where u_1 and u_2 are the instantaneous velocities at the exits of the opposed jets, and T_0 is the oscillation period of the modulation airflow. And for opposed jets formed by two excited jets with sinusoidal waveforms, the instantaneous velocity can be approximately expressed as

$$\begin{cases} u_1 = u_0 + A_0 \sin(2\pi f_0 t) \\ u_2 = u_0 + A_0 \sin(2\pi f_0 t + \pi) \end{cases} \tag{5}$$

To investigate the influence of TGP on the modulated jet, the velocity fluctuation of modulated jet with TGP was also measured. Figure 6 shows the time series and their power-frequency spectra of axial velocities. With TGP, the instantaneous fluctuation increases remarkably, but the frequency of the turbulent fluctuation is on the order of 10^3 Hz and is much higher than the excitation frequency. Even with TGP, the peak frequencies of the time series remain equal to the excitation frequencies, as indicated in Figures 6b, d.

Results

Flow patterns of jets with and without excitation

Some instantaneous photographs of smoke-seeded jets at various excitation frequencies are presented in Figure 7. For free jet shown in Figure 7a, a roll-up of the shear layer into vortex ring structures occurs at $x/D = 2.7$, and the resulting vortex ring structures are symmetric about the jet axis. The vortex structures break into small vortices at about $x/D = 8$ and the length of the potential core zone of the free jet is about $6D$. The formation frequency of the vortex ring is on the order of 100 Hz. For the forced jets, the vortex ring structures occur closer to the exit and have bigger size, as shown in Figure 7b. It can be observed that the formation frequencies of vortex rings of the forced jets are very close to their excitation frequencies. Some typical photos of smoke-seeded single jets with TGP are presented in Figures 7c, d. It can be observed that the order structures of the

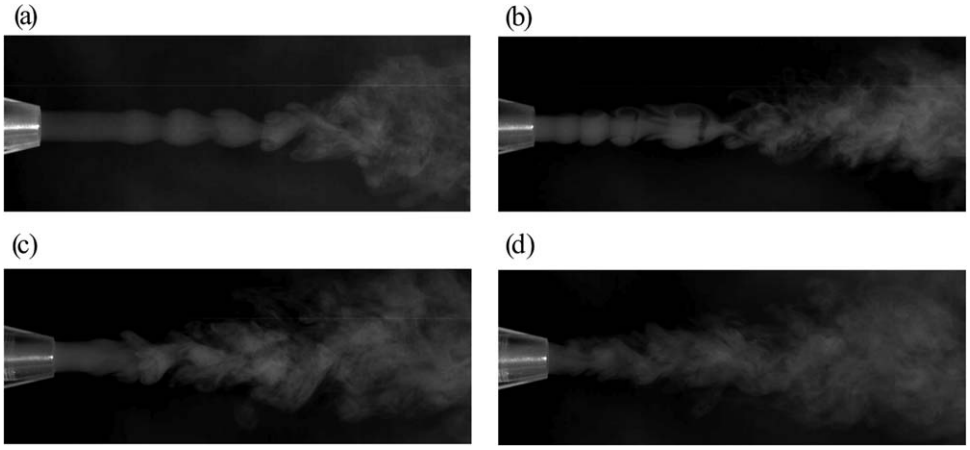

Figure 7. Smoke images of jets at $Re = 946$.

(a) Free jet, (b) $A_0/u_0 = 10\%$, and $f_0 = 1.0$ Hz, (c) $f_0 = 1.0$ Hz, $A_0/u_0 = 10\%$, and type A TGP, (d) $f_0 = 1.0$ Hz, $A_0/u_0 = 10\%$, and type B TGP.

forced jets are destroyed by high turbulence intensity. It also can be seen that the jet width increases remarkably with the increase of exit turbulence intensity.

Oscillation frequencies of opposed jets with excitations

At $L = 2D$, the impingement plane of opposed jets without excitation is located at the center between two opposing nozzles when we control the flow balance of opposed jets carefully. Under the excitation, it can be observed that the impingement plane oscillates periodically along the symmetry axis. Figure 8 represents the typical smoke images of modulated opposed jets at different moments. The five images in Figure 8 exactly correspond to the moments of 0, $1/4T$, $1/2T$, $3/4T$, and T in a full-oscillation period.

The time series of locations of the impingement planes of opposed jets with excitations were analyzed from the recorded smoke images. The time series of locations at $L = 2D$ and $f_0 = 1.0$, 8.4, and 25 Hz are plotted in Figure 9. The time series in Figure 9a corresponds to the smoke images in Figure 8. By FFT, we find the oscillation frequencies of the movement of the impingement planes in Figure 9 are 1.0, 8.3, and 24.5 Hz, which are very close to their excitation frequencies. It also can be seen that with the increase of excitation frequency, the oscillation amplitude of the impingement plane decreases dramatically from $1.40D$ to $0.14D$, and the cause will be elucidated later.

The oscillation frequencies of the impingement planes at various excitation frequencies and nozzle separations are shown in Figure 10. It can be seen that the normalized oscillation frequencies of the impingement planes fall in the range of 0.9–1.1, which indicates the impingement plane nearly synchronizes with the excitations. It can be deduced that if the fluctuation of the excitation is random, the movement of the impingement plane will be irregular, which might be cause for the irregular oscillation in the literature.[20,21]

It can be seen from Figures 8 and 9 that the impingement plane moves between two endpoints nearly with a uniform speed. So the mean movement velocity can be analyzed from the time series of locations of the impingement plane. The mean movement velocities of impingement planes at $Re = 946$ and $A_0/u_0 = 10\%$ are shown in Figure 11, in which the error bars mark the standard deviation of the data. It can be seen that u_{ip}/u_0 is in the range of 0.02–0.1 and decreases dramatically with increasing excitation frequency at $f_0 > 5$ Hz. The maximum velocity of impingement plane is close to A_0 and occurs at $2 \leq L/D \leq 8$ and $f_0 < 5$ Hz. More experimental results indicate that for opposed jets with excitation, the movement velocities are always close to or less than the excitation amplitudes.

Oscillation amplitude of opposed jets with excitation

Figure 12 sketches the oscillation amplitudes of impingement planes at $Re = 946$ and $A_0/u_0 = 10\%$. The oscillation

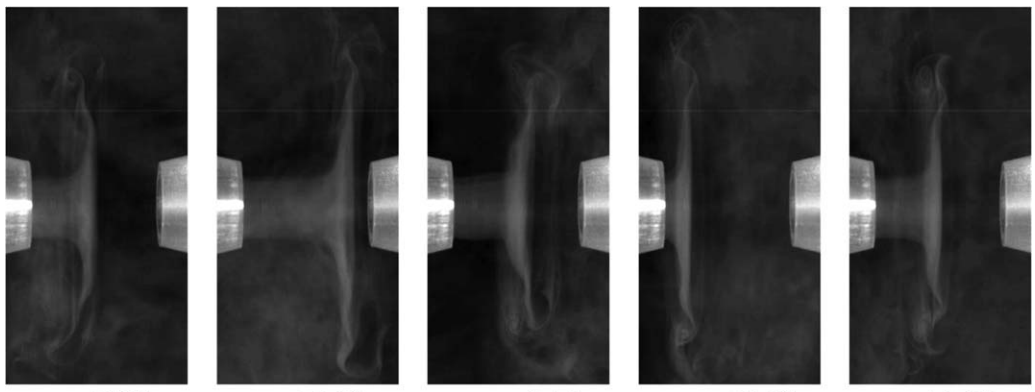

Figure 8. Smoke images of axisymmetric opposed jets at $Re = 946$, $L = 2D$, $A_0/u_0 = 10\%$, and $f_0 = 1.0$ Hz.

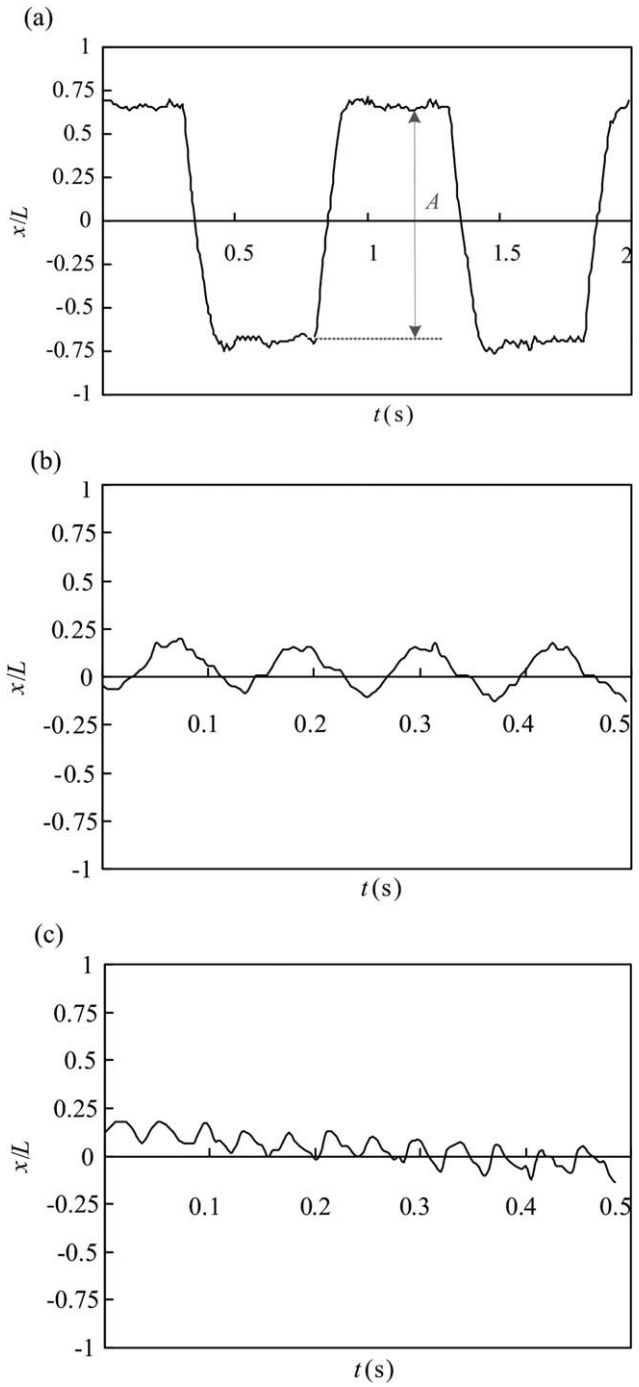

Figure 9. Time series of locations of impingement plane at $L = 2D$, $Re = 946$, and $A_0/u_0 = 10\%$.

(a) $f_0 = 1.0$ Hz, (b) $f_0 = 8.4$ Hz, and (c) $f_0 = 25.0$ Hz.

amplitude in the figure is the average of 15 oscillation periods, and the standard deviations are less than 10%. In the figure, the proportion of the height of rectangle to the height of square grid (A/L) represents the oscillation degree of the impingement plane. One can see that at all nozzle separations, the oscillation amplitudes decrease with the increase of excitation frequencies. It is interesting to see that there is a region (blue rectangle and background in Fig. 12) in which the impingement plane nearly reaches to the nozzle exits, and the oscillation is a full-scale amplitude oscillation. The full-amplitude oscillation occurs about at $2 \le L/D \le 8$ and

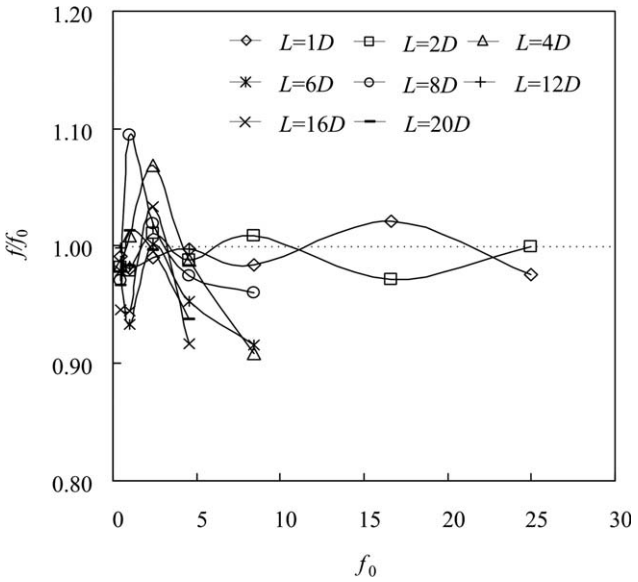

Figure 10. Oscillation frequencies of the impingement plane at $Re = 946$ and $A_0/u_0 = 10\%$.

$f_0 < 5$ Hz. At $L/D > 8$ or $L/D < 2$, the oscillation amplitude of the impingement plane decreases gradually.

The sketch of the oscillation amplitudes of impingement planes at $Re = 6624$ and $A_0/u_0 = 20\%$ is plotted in Figure 13. It can be seen that with the increase of excitation amplitudes and exit bulk velocities, the oscillation amplitudes increase, and the region with full amplitude oscillation also appears in the range of $2 \le L/D \le 8$, but the range of excitation frequency corresponding to full-amplitude oscillation is extended largely.

The influence of exit turbulence intensity on the oscillation amplitude of the impingement plane was also investigated by adding TGP in the nozzles. The comparisons of oscillation amplitudes of the impingement plane of modulated opposed jets with various exit turbulence intensities are shown in Figure 14. It can be seen that with the increase of exit turbulence intensity, the oscillation amplitude decreases remarkably at $L \ge 4D$ and the oscillation tends to disappear at $L > 8D$.

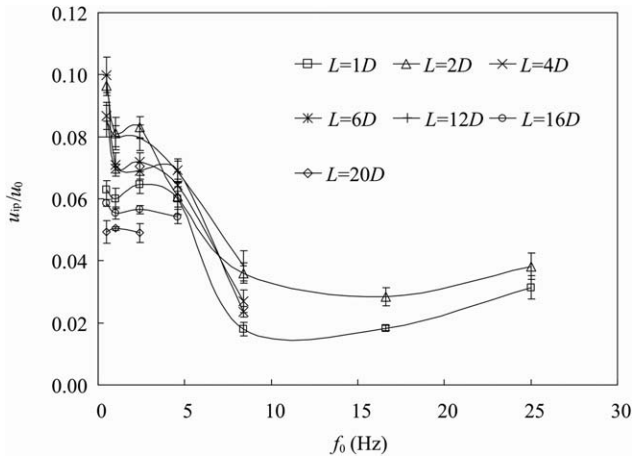

Figure 11. Normalized movement velocities of the impingement plane at $Re = 946$ and $A_0/u_0 = 10\%$.

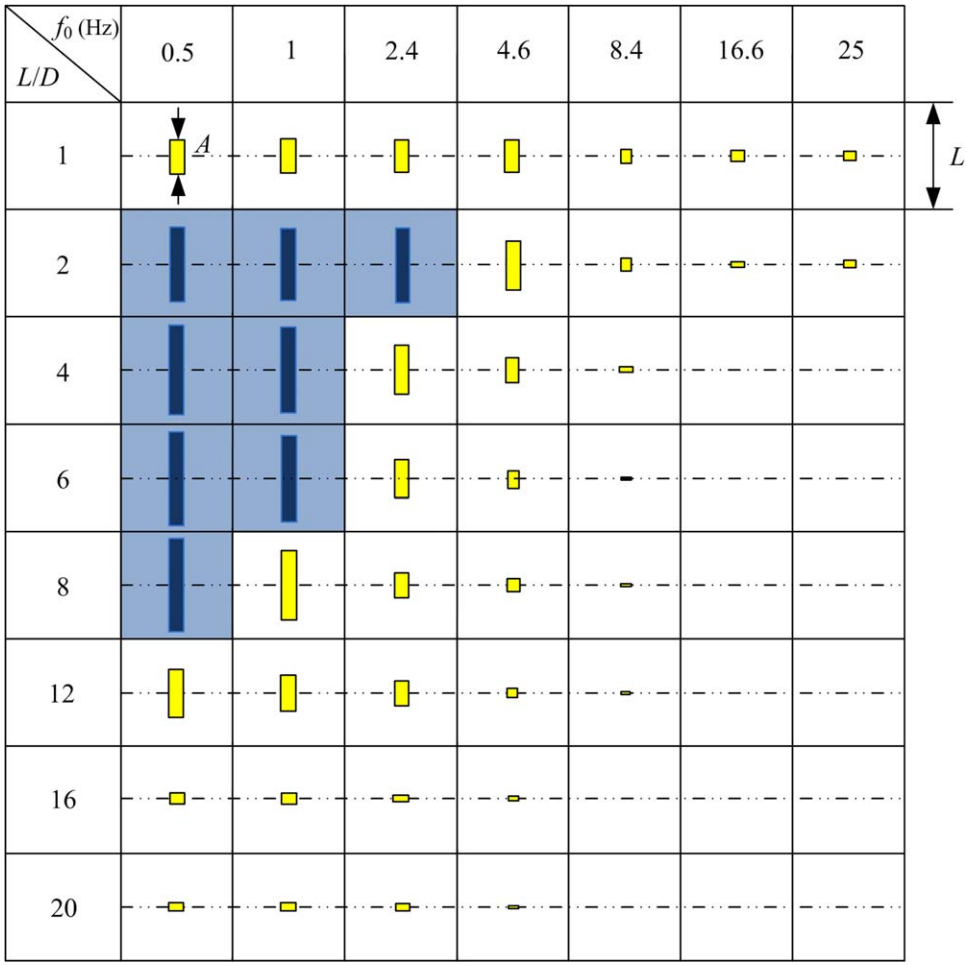

Figure 12. Normalized oscillation amplitudes of the impingement plane at $Re = 946$ and $A_0/u_0 = 10\%$.

[Color figure can be viewed in the online issue, which is available at wileyonlinelibrary.com.]

Discussion

Due to the difference of the inflow and boundary conditions, a direct comparison of current study with the results in the literature is difficult. It must be pointed out first that the self-sustained chaotic oscillation in RIM is related to the confined boundary condition,[15–19] which is different to the low-frequency periodic oscillation of axisymmetric opposed jets with excitations. Second, current results can be used to explain the low-frequency irregular oscillations reported in the experiments[20,21] but absent in the simulation and stability analysis.[13,14] This discrepancy is due to the different boundary conditions, because the velocity inlet in the simulation is laminar and constant, while the flow fluctuations and other disturbance more or less exist in experiments. This discrepancy also occurred in the DNS of Icardi et al.[31] and they suggested that some small excitation oscillations similar to the experimental ones should be introduced in inflow conditions in the simulation of opposed jets. Moreover, the experimental results of the planar opposed jets with acoustic excitation in our lately published paper show that the planar opposed jets exhibit a self-sustained deflecting oscillation and the impinging plane do not synchronize with the excitation until the excitation amplitude is larger than 30%, which proves once again the flow regimes of planar opposed jets and axisymmetric opposed jets are different in nature.[21–23,35]

As discussed in the introduction, the stagnation point offset or the three stable states are the inborn instability regimes of axisymmetric opposed jets,[3–12] which are the prerequisites of the excited oscillation in current article. But the excitation of modulated airflow is the direct cause of the periodic oscillation of the impinging plane of axisymmetric opposed jets under excitations, and current experimental results indicate that the excitation frequency, excitation amplitude, turbulence intensity, and nozzle separation have important influence on the periodic oscillation of opposed jets with excitations. The influences of these parameters on the oscillation behaviors are essentially attributed to the movement speed of the impingement plane and the axial velocity gradient of axisymmetric opposed jets.

The movements of the impingement plane are mainly caused by the momentum imbalance of opposed jets at the stagnation point. When the velocity fluctuations of two modulated opposed jets have a phase displacement, their instantaneous velocities and momenta when they are colliding are not equal. The maximum difference of instantaneous velocity is nearly equal to the excitation amplitude. The difference of instantaneous velocities and momenta will cause the movement of the impingement plane. If the impingement plane can move from one jet exit to another jet exit in half a period, then it has a full-amplitude oscillation. The following equations can be used to estimate the displacement (Δx) of the impingement plane in half a period

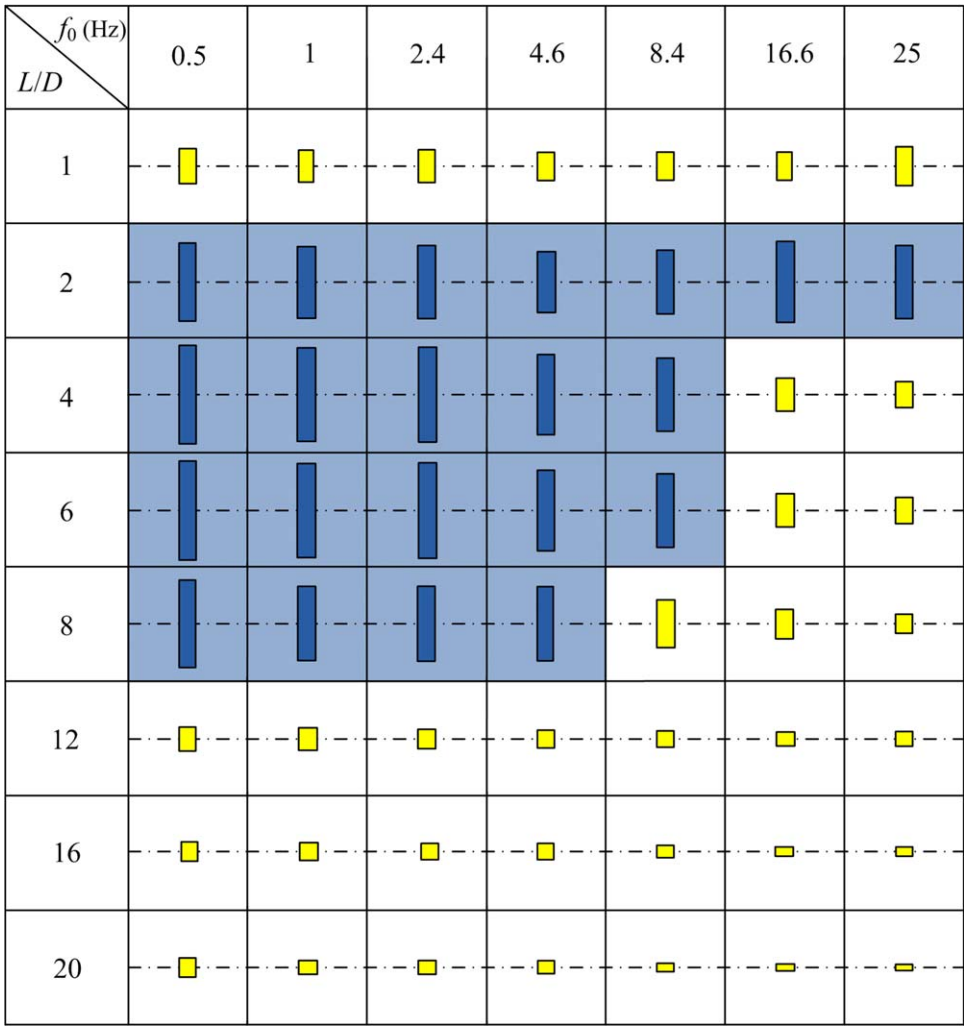

Figure 13. Normalized oscillation amplitudes of the impingement plane at $Re = 6624$ and $A_0/u_0 = 20\%$.

[Color figure can be viewed in the online issue, which is available at wileyonlinelibrary.com.]

$$\Delta x = \frac{u_{ip}}{2f_0}, \text{ or } \Delta x/L = \frac{u_{ip}}{2L \cdot f_0} \tag{6}$$

According to the relationship of $u_{ip} \leq A_0$ indicated in Figure 11, above equations can be written as

$$\Delta x \leq \frac{A_0}{2f_0}, \text{ or } \Delta x/L \leq \frac{A_0}{2L \cdot f_0} \tag{7}$$

Above equations indicate that the oscillation amplitudes of opposed jets with excitation decrease with the excitation frequency and increase with the excitation amplitude and the movement velocity of the impingement plane, so the full-amplitude oscillation will occurs at low-excitation frequency, which is in reasonable agreement with the results in Figures 12 and 13. It should be pointed out that Eqs. 6 and 7 are established on the prerequisites of $f \approx f_0$ and $u_{ip} \leq A_0$, which have been validated by experimental results in Figures 10 and 11, respectively. These equations are valid for axisymmetric opposed jets, but maybe not true for planar opposed jets or other similar flows.[35]

The influence of TGP on the oscillation amplitude of opposed jets also results from the change of the movement velocity of the impingement plane. At first, the high frequency turbulence fluctuation caused by TGP will decrease the instantaneous velocity difference of the opposed jets, as shown in Figure 6. Moreover, it can be seen from Figure 7 that the jet width and axial velocity gradient increase with the exit turbulent intensity, so the movement velocity of the impingement plane will decrease, which also results in the decrease of the oscillation amplitude, as indicated in Figure 14. It should be pointed out that in Figure 11, the remarkable decrease of u_{ip} at $f_0 \geq 5$ Hz is partly due to the change of the waveform of the modulated jets. As shown in Figure 5, the instantaneous velocity curve of the modulated jets becomes like a sinusoidal wave at $f_0 > 5$ Hz, which cause the decrease of instantaneous velocity difference as the opposed jets collide. So, the movement speed and oscillation amplitude decrease at $f_0 > 5$ Hz, as shown in Figures 11, 12, and 13.

Though the movement velocity of impingement plane is mainly determined by the oscillation amplitude of the modulated jets, it is also affected by the axial velocity gradient at different nozzle separations. The flow field of turbulent opposed jets can be divided into three regions, which are the free jet zone (the region keeps the characteristics of free jet and this zone is absent at $L/D < 2$), impingement zone, and radial jet zone.[10] With the increase of nozzle separation, the collision region will change from the potential core region to the developing region of the jets, as shown in Figures 7a, b. The flow regimes of opposed jets at different nozzle separation ranges can be summarized as follows:

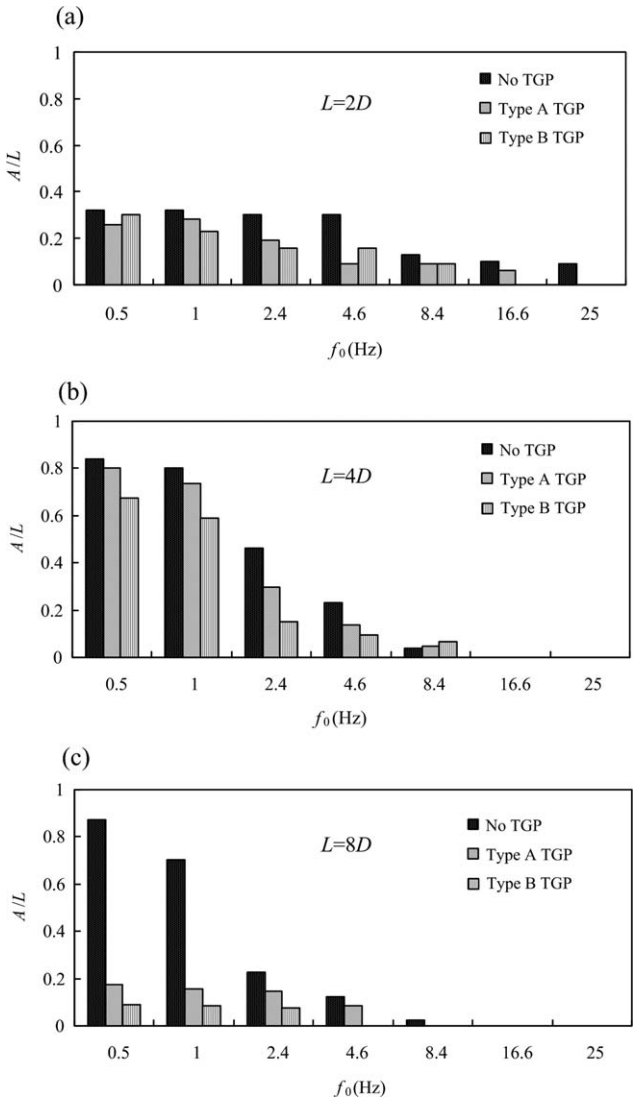

Figure 14. Influence of turbulence generating plates on the oscillation amplitude of impingement planes at $Re = 946$ and $A_0/u_0 = 10\%$.

1. At $L/D < 2$ or $L/D > 8$, opposed jets collide each other in a zone with very high axial velocity gradient, and the velocities of the opposing jets before they are impinging are less than their initial exit velocities, so the movement velocity of the impingement plane will be less than A_0. Moreover, the movement of the impingement plane will encounter some resistance cause by the axial velocity gradient, so the resultant oscillation amplitude will decrease, as shown in Figure 11.

2. About at $2 \leq L/D \leq 8$, the collision of the opposed jets occurs in the potential core zone and the axial velocity gradient is very low except in the impingement zone. The velocities of the opposing jets before they are impinging are nearly equal to their initial exit velocities, and the instantaneous velocities difference is close to A_0. This axial velocity distribution means the stagnation point or the impingement plane can move smoothly along the symmetric axis from one nozzle exit to another, and cannot resist any small axial velocity imbalance or fluctuation. This is why the full-amplitude oscillation tends to take place at $2 \leq L/D \leq 8$, just as shown in Figures 12 and 13. Similarly, the stagnation point is also very sensitive to the little difference of the exit velocities of the opposed jets at $2 \leq L/D \leq 8$, just as the conclusions reported in our previous work.[10,11]

It can be seen from our previous studies[10–12] and current experimental results that both the stagnation point offset and the oscillation of the impingement plane are essentially caused by the exit velocity difference or fluctuations of the opposed jets. The exit velocity imbalance of opposed jets results in the stagnation point offset, while the periodic fluctuation exit velocity causes the axial periodic oscillation, and the oscillation frequency is almost equal to the excitation frequency.

Conclusions

To successfully exploit opposed jets for engineering applications, it is very necessary to study the flow regimes. In current study, the periodic oscillations of axisymmetric turbulent opposed jets under modulated airflow were investigated experimentally. Results show the impingement plane synchronizes with the excitation and the excitation frequency, excitation amplitude, and axial velocity gradient have substantial influences on the oscillation amplitude of the excited oscillation. The movement of the impingement plane is subject to the low-frequency excitation and its oscillation amplitude decreases with the increase of the excitation frequency. For axisymmetric opposed jets, the mean movement velocity of the impingement plane is always close to or less than the excitation amplitude of the modulation. High exit turbulence intensity decreases the oscillation amplitude of opposed jets with excitation.

Current experiments provide a useful method to control or excite the dynamics behaviors of turbulent opposed jets, with which we can improve the mixing and enhance the heat- and mass-transfer in impinging jet reactors. The results in current study present a significant contribution to the knowledge of the intrinsic mechanism of turbulent opposed jets. The results will also provide a sound basis for the future computational fluid dynamics simulation and stability analysis of turbulent opposed jets.

Acknowledgments

This study was supported by the National Development Programming of Key Fundamental Researches of China (2010CB227004), the National Natural Science Foundation of China (20906024), and the Fundamental Research Funds for the Central Universities (WB1014022). Especially, we express our sincere thanks to the anonymous reviewers for their helpful suggestions on the quality improvement of the paper.

Literature Cited

1. Elperin IT. Heat and mass transfer in opposing currents (in Russian). *J Eng Phys*. 1961;6:62–68.
2. Tamir A. *Impinging Streams Reactors: Fundamentals and Applications*. Amsterdam: Elsevier, 1994.
3. Rolon JC, Veynante D, Martin JP. Counter jet stagnation flows. *Exp Fluids*. 1991;11:313–324.
4. Kostiuk LW, Bray KNC, Cheng RK. Experimental study of premixed turbulent combustion in opposed streams. Part I-nonreacting flow field. *Combust Flame*. 1993;92:377–395.
5. Ogawa N, Maki H. Studies on opposed turbulent jets, (influences of a body on the axis of opposed turbulent jets). *Bull JSME*. 1986;29:2872–2877.
6. Ogawa N, Maki H, Hijikata K. Studies on opposed turbulent jets, (impact position and turbulent component in jet center). *Int J JSME*. 1992;35:205–217.

7. Korusoy E, Whitelaw JH. Extinction and relight in opposed flames. *Exp Fluids*. 2002;33:75–89.
8. Lindstedt RP, Luff DS, Whitelaw JH. Velocity and strain-rate characteristics of opposed isothermal flows. *Flow Turbul Combust*. 2005; 74:169–194.
9. Coppola G, Gomez A. Experimental study of highly turbulent isothermal opposed-jet flows. *Phys Fluids*. 2010;22:105101–105116.
10. Li WF, Sun ZG, Liu HF, Wang FC, Yu ZH. Experimental and numerical study on stagnation point offset of turbulent opposed jets. *Chem Eng J*. 2008;138:283–294.
11. Li WF, Yao TL, Wang FC. Study on factors influencing stagnation point offset of turbulent opposed jets. *AIChE J*. 2010;56:2513–2522.
12. Sun ZG, Li WF, Liu HF. Stagnation point offset of two opposed jets. *Ind Eng Chem Res*. 2010;49:5877–5883.
13. Pawlowski RP, Salinger AG, Shadid JN, Mountziaris TJ. Bifurcation and stability analysis of laminar isothermal counterflowing jets. *J Fluid Mech*. 2006;551:117–139.
14. Ciani A, Kreutner W, Frouzakis CE, Lust K, Coppola G, Boulouchos K. An experimental and numerical study of the structure and stability of laminar opposed-jet flows. *Comput Fluids*. 2010;39: 114–124.
15. Wood PE, Hrymak A, Yeo R, Johnson DA, Tyagi A. Experimental and computational studies of the fluid mechanics in an opposed jet mixing head. *Phys Fluids A*. 1991;3:1362–1368.
16. Johnson DA, Wood PE. Self-sustainable oscillations in opposed impinging jets in an enclosure. *Can J Chem Eng*. 2000;78:867–875.
17. Teixeira AM, Santos RJ, Costa MRPFN, Lopes JCB. Hydrodynamics of the mixing head in RIM: LDA flow-field characterization. *AIChE J*. 2005;51:1608–1619.
18. Santos RJ, Erkoç E, Dias MM, Teixeira AM, Lopes JCB. Hydrodynamics of the mixing chamber in RIM: PIV flow-field characterization. *AIChE J*. 2008;54:1153–1163.
19. Santos RJ, Erkoç E, Dias MM, Lopes JCB. Dynamic behavior of the flow field in a RIM machine mixing chamber. *AIChE J*. 2009;55: 1338–1351.
20. Stan G, Johnson DA. Experimental and numerical analysis of turbulent opposed impinging jets. *AIAA J*. 2001;39:1901–1908.
21. Li WF, Yao TL, Liu HF, Wang FC. Experimental investigation of flow regimes of axisymmetric and planar opposed jets. *AIChE J*. 2011;57:1434–1445.
22. Denshchikov VA, Kontratev VN, Romashev AN. Interaction between two opposed jets. *Fluid Dyn*. 1978;13:924–926.
23. Denshchikov VA, Kontratev VN, Romashev AN, Chubarov VM. Auto-oscillations of planar colliding jets. *Fluid Dyn*. 1983;18:460–462.
24. Okkels F, Tabeling P. Spatiotemporal resonances in mixing of open viscous fluids. *Phys Rev Lett*. 2004;92:038301–038304.
25. Ito Y, Komori S. A vibration technique for promoting liquid mixing and reaction in a microchannel. *AIChE J*. 2006;52:3011–3017.
26. Li J, Aranson IS, Kwok WK, Tsimring LS. Periodic and disordered structures in a modulated gas-driven granular layer. *Phys Rev Lett*. 2003;90:134301.
27. Chauhan A, Maldarelli C, Rumschitzki DS, Papageorgiou DT. An experimental investigation of the convective instability of a jet. *Chem Eng Sci*. 2003;58:2421–2432.
28. Fujii T, Sando Y, Higashino K, Fujii Y. A plug and play microfluidic device. *Lab Chip*. 2003;3:193–197.
29. Sun CL, Sie JY. Active mixing in diverging microchannels. *Microfluid Nanofluid*. 2010;8:485–495.
30. Erkoç E, Santos RJ, Dias MM, Lopes JCB. Enhancing the RIM process with pulsation technology: CFD study. In: Proceedings of European congress of chemical engineering(ECCE-6). Copenhagen, September 16–20, 2007.
31. Icardi M, Gavi E, Marchisio DL, Barresi AA, Olsen MG, Fox RO, Lakehal D. Investigation of the flow field in a three-dimensional Confined Impinging Jets Reactor by means of microPIV and DNS. *Chem Eng J*. 2011;166:294–305.
32. Qiu SX, Xu P, Jiang ZT, Mujumdar AS. Numerical modeling of pulsed laminar opposed impinging jets. *Eng Appl Comp Fluid*. 2012; 6:195–202.
33. Coppola G, Gomez A. Experimental investigation on a turbulence generation system with high-blockage plates. *Exp Therm Fluid Sci*. 2009;33:1037–1048.
34. Jørgensen FE. *How to Measure Turbulence with Hot-Wire Anemometers—A Practical Guide*. Denmark: Dantec Dynamics, 2002;33–44.
35. Li WF, Huang GF, Tu GY, Liu HF, Wang FC. Experimental study of planar opposed jets with acoustic excitation. *Phys Fluids*. 2013; 25:014108–014123.

Manuscript received Nov. 18, 2012, revision received Apr. 24, 2013, and final revision received Jul. 3, 2013.